Role of spectral non-idealities in the design of solar thermophotovoltaics

Citation: Lenert, Andrej, Youngsuk Nam, David M. Bierman, and Evelyn N. Wang. "Role of Spectral Non-Idealities in the Design of Solar Thermophotovoltaics." Optics Express 22, no. S6 (2014): A1604.

As Published: http://dx.doi.org/10.1364/OE.22.0A1604

Publisher: Optical Society of America

Persistent URL: http://hdl.handle.net/1721.1/93172

Version: Author's final manuscript: final author's manuscript post peer review, without publisher's formatting or copy editing

DOI: 10.1364/OE.22.0A1604
SOURCE: Lenert, Andrej, Youngsuk Nam, David M. Bierman, and Evelyn N. Wang. "Role of Spectral Non-Idealities in the Design of Solar Thermophotovoltaics." Optics Express 22, no. S6, A1604, 2014.

Role of spectral non-idealities in the design of solar thermophotovoltaics

Andrej Lenert,[1,2] Youngsuk Nam,[3] David M. Bierman,[1] and Evelyn N. Wang[1,*]

[1]Department of Mechanical Engineering, Massachusetts Institute of Technology, 77 Massachusetts Avenue, Cambridge, Massachusetts, USA, [2]Department of Mechanical Engineering, 2350 Hayward Street, University of Michigan, Ann Arbor, Michigan, USA, [3]Department of Mechanical Engineering, Kyung Hee University, Yongin, 446-701, Korea
[*]enwang@mit.edu

Abstract: To bridge the gap between theoretically predicted and experimentally demonstrated efficiencies of solar thermophotovoltaics (STPVs), we consider the impact of spectral non-idealities on the efficiency and the optimal design of STPVs over a range of PV bandgaps (0.45-0.80 eV) and optical concentrations (1-3,000x). On the emitter side, we show that suppressing or recycling sub-bandgap radiation is critical. On the absorber side, the relative importance of high solar absorptance versus low thermal emittance depends on the energy balance. Both results are well-described using dimensionless parameters weighting the relative power density above and below the cutoff wavelength. This framework can be used as a guide for materials selection and targeted spectral engineering in STPVs.

OCIS codes: (350.6050) Solar energy; (220.0220) Optical design and fabrication; (350.4238) Nanophotonics and photonic crystals.

References and links

1. N.-P. Harder and P. Würfel, "Theoretical limits of thermophotovoltaic solar energy conversion," Semicond. Sci. Technol. **18**, 151-156 (2003).
2. A. Datas and C. Algora, "Development and experimental evaluation of a complete solar thermophotovoltaic system," Prog. Photovolt: Res. Appl. **21**, 1025-1039 (2013).
3. A. Lenert, D. M. Bierman, Y. Nam, W. R. Chan, I. Celanovic, M. Soljacic, and E. N. Wang, "A nanophotonic solar thermophotovoltaic device," Nat. Nano. **9**, 126-130 (2014).
4. V. Rinnerbauer, A. Lenert, D. M. Bierman, Y. X. Yeng, W. R. Chan, R. D. Geil, J. J. Senkevich, J. D. Joannopoulos, E. N. Wang, M. Soljačić, and I. Celanovic, "Metallic photonic crystal absorber-emitter for efficient spectral control in high-temperature solar thermophotovoltaics," Adv. Energ. Mater. **4**, (2014).
5. P. Bermel, J. Lee, J. D. Joannopoulos, I. Celanovic, and M. Soljacic, "Selective solar absorbers," Annu. Rev. Heat Transfer **15**, (2012).
6. V. Rinnerbauer, S. Ndao, Y. X. Yeng, W. R. Chan, J. J. Senkevich, J. D. Joannopoulos, M. Soljacic, and I. Celanovic, "Recent developments in high-temperature photonic crystals for energy conversion," Energy Environ. Sci. **5**, 8815-8823 (2012).
7. V. Rinnerbauer, Y. X. Yeng, W. R. Chan, J. J. Senkevich, J. D. Joannopoulos, M. Soljacic, and I. Celanovic, "High-temperature stability and selective thermal emission of polycrystalline tantalum photonic crystals," Opt. Express **21**, 11482-11491 (2013).
8. V. Rinnerbauer, S. Ndao, Y. Xiang Yeng, J. J. Senkevich, K. F. Jensen, J. D. Joannopoulos, M. Soljacic, I. Celanovic, and R. D. Geil, "Large-area fabrication of high aspect ratio tantalum photonic crystals for high-temperature selective emitters," J. Vac. Sci. Technol. B **31**, 011802-011807 (2013).
9. K. A. Arpin, M. D. Losego, A. N. Cloud, H. Ning, J. Mallek, N. P. Sergeant, L. Zhu, Z. Yu, B. Kalanyan, G. N. Parsons, G. S. Girolami, J. R. Abelson, S. Fan, and P. V. Braun, "Three-dimensional self-assembled photonic crystals with high temperature stability for thermal emission modification," Nat. Commun. **4**, (2013).
10. W. Shockley and H. J. Queisser, "Detailed balance limit of efficiency of p-n junction solar cells," J. Appl. Phys. **32**, 510-519 (1961).
11. M. Röger, C. Rickers, R. Uhlig, F. Neumann, and C. Polenzky, "Infrared-reflective coating on fused silica for a solar high-temperature receiver," J. Sol. Energ. **131**, 021004-021004 (2009).

DOI: 10.1364/OE.22.0A1604
SOURCE: Optics Express 22, no. S6, A1604, 2014.

12. T. D. Rahmlow, D. M. DePoy, P. M. Fourspring, H. Ehsani, J. E. Lazo-Wasem, and E. J. Gratrix, "Development of front surface, spectral control filters with greater temperature stability for thermophotovoltaic energy conversion," AIP Conf. Proc. **890**, 59-67 (2007).
13. P. M. Fourspring, D. M. DePoy, T. D. Rahmlow Jr, J. E. Lazo-Wasem, and E. J. Gratrix, "Optical coatings for thermophotovoltaic spectral control," Appl. Opt. **45**, 1356-1358 (2006).
14. J. B. Chou, Y. X. Yeng, A. Lenert, V. Rinnerbauer, I. Celanovic, M. Soljacic, E. N. Wang, and S.-G. Kim, "Design of wide-angle selective absorbers/emitters with dielectric filled metallic photonic crystals for energy applications," Opt. Express **22**, A144-A154 (2014).
15. J. B. Chou, Y. X. Yeng, Y. E. Lee, A. Lenert, V. Rinnerbauer, I. Celanovic, M. Soljačić, N. X. Fang, E. N. Wang, and S.-G. Kim, "Enabling ideal selective solar absorption with 2D metallic dielectric photonic crystals," Adv. Mats., (2014).
16. Y. X. Yeng, J. B. Chou, V. Rinnerbauer, Y. Shen, S.-G. Kim, J. D. Joannopoulos, M. Soljacic, and I. elanovi, "Global optimization of omnidirectional wavelength selective emitters/absorbers based on dielectric-filled anti-reflection coated two-dimensional metallic photonic crystals," Opt. Express **22**, 21711-21718 (2014).
17. P. Bermel, M. Ghebrebrhan, W. Chan, Y. X. Yeng, M. Araghchini, R. Hamam, C. H. Marton, K. F. Jensen, M. Soljacic, J. D. Joannopoulos, S. G. Johnson, and I. Celanovic, "Design and global optimization of high-efficiency thermophotovoltaic systems," Opt. Express **18**, A314-A334 (2010).
18. Y. Nam, Y. X. Yeng, A. Lenert, P. Bermel, I. Celanovic, M. Soljačić, and E. N. Wang, "Solar thermophotovoltaic energy conversion systems with two-dimensional tantalum photonic crystal absorbers and emitters," Sol. Energ. Mater. **122**, 287-296 (2014).
19. E. Rephaeli and S. Fan, "Absorber and emitter for solar thermo-photovoltaic systems to achieve efficiency exceeding the shockley-queisser limit," Opt. Express **17**, 15145-15159 (2009).
20. C. Wu, I. Burton Neuner, J. John, A. Milder, B. Zollars, S. Savoy, and G. Shvets, "Metamaterial-based integrated plasmonic absorber/emitter for solar thermo-photovoltaic systems," J. Opt. **14**, 024005 (2012).
21. R. Siegel and J. R. Howell, *Thermal Radiation Heat Transfer* (Hemisphere Pub. Corp., 1981).
22. M. F. Modest, *Radiative Heat Transfer* (Academic Press, 2013).
23. S. V. Boriskina and G. Chen, "Exceeding the solar cell shockley–queisser limit via thermal up-conversion of low-energy photons," Opt. Comm. **314**, 71-78 (2014).
24. D. Kraemer, B. Poudel, H.-P. Feng, J. C. Caylor, B. Yu, X. Yan, Y. Ma, X. Wang, D. Wang, A. Muto, K. McEnaney, M. Chiesa, Z. Ren, and G. Chen, "High-performance flat-panel solar thermoelectric generators with high thermal concentration," Nat. Mater. **10**, 532-538 (2011).
25. G. Chen, "Theoretical efficiency of solar thermoelectric energy generators," J. Appl. Phys. **109**, 104908 (2011).
26. M. Telkes, "Solar thermoelectric generators," J. Appl. Phys. **25**, 765-777 (1954).
27. P. Bermel, M. Ghebrebrhan, M. Harradon, Y. Yeng, I. Celanovic, J. Joannopoulos, and M. Soljacic, "Tailoring photonic metamaterial resonances for thermal radiation," Nano. Res. Let. **6**, 549 (2011).

1. Introduction

Solar thermophotovoltaic (STPV) power generation relies on an intermediate material, an absorber-emitter, situated between the sun and a photovoltaic cell (PV). This material converts the broad solar spectrum into heat before tuning the thermal emission such that only useful radiation is delivered to the PV cell. Theoretical studies predict that solar-to-electrical efficiencies can approach 85% for STPVs [1]. The efficiencies of experimentally demonstrated STPVs, on the other hand, remain below 5% [2-4]. The large discrepancy between these two realms is in large part due to spectral non-idealities and parasitic losses; we broadly define a spectral non-ideality as a deviation with respect to the emittance profile of an ideal spectrally-selective surface.

Spectrally-engineered surfaces can be used as both absorbers, to efficiently collect sunlight, and as emitters, to selectively emit useful radiation towards a PV cell. Here we focus on the spectral features of the STPV components and not on the directional features such that we assume the spectral properties to be isotropic ($\varepsilon_{\lambda,\theta} \approx \varepsilon_\lambda$) and to obey Kirchhoff's law, *i.e.*, $\alpha_\lambda = \varepsilon_\lambda$. For wavelength selective absorbers, the cut-off wavelength ($\lambda_{c,absorber} = \lambda_c$) and the spectral properties optimize absorption (high ε_λ) of short-wavelength concentrated sunlight ($\lambda<\lambda_c$), and suppress re-emission (low ε_λ) of long-wavelength thermal radiation ($\lambda>\lambda_c$). On the emitter side, the cutoff wavelength coincides with the PV bandgap (E_g), *i.e.*, $\lambda_{c,emitter} = \lambda_g = hc/E_g$ where h is Planck's constant and c is the speed of light in vacuum. The spectral properties enhance thermal emission of useful radiation ($\lambda<\lambda_g$) while suppressing sub-bandgap radiation ($\lambda>\lambda_g$). Current state-of-the-art spectrally-engineered surfaces compatible with the

DOI: 10.1364/OE.22.0A1604
SOURCE: Optics Express 22, no. S6, A1604, 2014.

high operating temperatures of STPVs have tunable cutoff wavelengths with an average emittance of ~0.80 at wavelengths below the cutoff and ~0.20 at wavelengths above the cutoff [4-9]. Compared to an ideal selective surface, these properties represent approximately a 0.20 non-ideality. In this work, the spectral non-idealities are generalized into the following [see Fig. 1]: δ_h^a – the absorber-side deviation from unity absorptance for $\lambda<\lambda_c$ (the emittance is 1- δ_h^a in that region), δ_l^a – the absorber-side deviation from zero emittance for $\lambda>\lambda_c$, δ_h^e – the emitter-side deviation from unity emittance for $\lambda<\lambda_g$, and δ_l^e – the emitter-side deviation from zero sub-bandgap emittance for $\lambda>\lambda_g$.

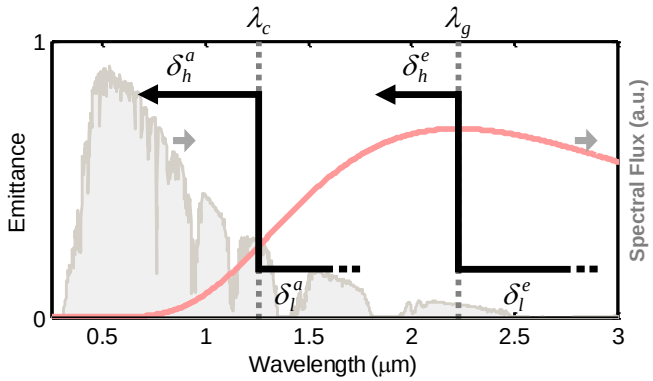

Fig. 1. Generalized spectral non-idealities: deviations from unity emittance at wavelengths below the cutoff (δ_h) and from zero emittance above the cutoff (δ_l) on both the absorber (*a*) and the emitter (*e*) side. The following spectral fluxes are shown for reference: AM 1.5D with 40x concentration (gray) and blackbody emission at 1300 K (light red).

Despite the remarkable properties and the tunability of the state-of-the-art surfaces, a 0.20 level of spectral non-ideality hinders STPV power generation from reaching high efficiencies (*i.e.*, exceeding the Shockley-Queisser limit [10] at moderate optical concentrations on the order of 1000x and below) as evidenced by previous experimental results and our subsequent analysis. To achieve high efficiencies, improved spectral control is needed. This second level of control may come in the form of selective windows/filters and/or improved selective absorber/emitter surfaces. Selective windows allow solar radiation to pass while reflecting thermal emission back to the absorber. Selective windows have been demonstrated with solar-weighted transmittance exceeding 0.80 and thermal reflectance of approximately 0.50 (weighted for a ~1400 K blackbody) [11]. Similarly, sub-bandgap reflecting filters allow useful ($\lambda<\lambda_g$) radiation to pass while reflecting sub-bandgap ($\lambda>\lambda_g$) radiation back to the emitter. Tandem filters (interference + plasma filter) with thermally-averaged (1300 K) reflectance exceeding 0.95 at wavelengths above λ_g and 0.60-0.85 transmittance below λ_g have been demonstrated [12, 13]. Through a stacked configuration of a surface and a selective window/filter [see Fig. 2], it is expected that spectral non-idealities at wavelengths above the cutoff can be reduced significantly. On the other hand, surface engineering can result in increased emittance at wavelengths below the cutoff; for example, a dielectric can be used to fill the cavities of a two-dimensional metallic photonic crystal [14-16].

Although interference filters and nanophotonic surfaces allow us to engineer the properties with a certain degree of tunability and temperature-independence, tradeoffs between high transmittance/absorptance in one part of the spectrum and high reflectance in another part are inevitable. Therefore, uniformly decreasing the spectral non-idealities by one order of magnitude (from ~0.10 to ~0.01) is difficult to achieve and possibly unnecessary. In practice, it is important to understand what spectral properties have the most impact on improving the efficiency of the system from its current level of non-idealities.

DOI: 10.1364/OE.22.0A1604
SOURCE: Optics Express 22, no. S6, A1604, 2014.

This work presents a simple framework that determines which spectral properties are critical for improving the STPV efficiency and should be targeted using either additional components (windows/filters) or spectral engineering. An additional component or photonic design can be globally optimized [17-19] by coupling electromagnetic solvers for structured surfaces with a full STPV thermo-electrical model, however, there is currently little guidance regarding the initial materials selection or design space. We first present the sensitivity of the performance and the optimal design to generalized spectral non-idealities. Then, we suggest physically-meaningful dimensionless quantities which can be used as weighting factors or figures-of-merit to guide the selection of materials and the design of nanophotonic surfaces for improved STPV efficiency.

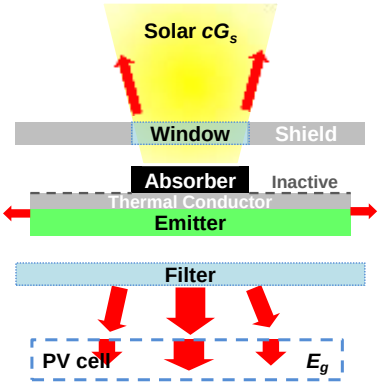

Fig. 2. Schematic of a planar STPV device and its components. The window and the absorber are grouped together as "absorber-side". The emitter and the filter are grouped together as "emitter-side". The model accounts for parasitic losses from the inactive area and the mechanical supports.

2. Model: STPV with generalized non-idealities

Our model is based on previous STPV models [19, 20], however, instead of considering a specific absorber-emitter design, we consider a generalized absorber-emitter with non-idealities. We also consider the presence of realistic parasitic losses through the hot inactive area and the mechanical supports. In developing the model, several simplifying assumptions were made that may underestimate or overestimate the system performance, as discussed below. Nevertheless, our focus was not on the ultimate efficiency of the system but on the relative influence of the spectral non-idealities on the optimal system design.

The model accounts for the following: the actual AM 1.5D solar spectrum (appropriate for concentrated solar applications), an absorber and an emitter with non-idealities on either side of their respective sharp cutoff wavelengths [shown in Fig. 1], and non-ideal cell behavior (*i.e.*, non-radiative recombination). A steady-state energy balance is implemented at the absorber-emitter to determine its operating temperature:

$$\sigma(T_{ae}^4 - T_{amb}^4)(\bar{\varepsilon}_a A_a + \bar{\varepsilon}_e A_e + \bar{\varepsilon}_{na}^{eff} |A_e - A_a|) + Q_{parasitic} = \bar{\alpha}_a A_a c G_s \quad (1)$$

where σ is Stefan's constant, T_{ae} is the temperature of the absorber-emitter (assumed to be isothermal), T_{amb} is the ambient temperature (*i.e.*, 300 K), $\bar{\varepsilon}$ is the thermally weighted emittance, $\bar{\alpha}$ is the solar weighted absorptance, G_s is the nominal solar flux (1000 W/m^2 = 1 sun), $Q_{\text{parasitic}}$ is the heat loss to the mechanical supports, c is the level of optical concentration, and A is the area of the component (*a*—absorber, *e*—emitter). In the above formulation of the energy balance, we assume that the absorber, the emitter, and the inactive area only "see" the environment, the PV cell, and the shield, respectively. The assumption is valid as long as the characteristic length scale of the components (L) is much larger than the gap spacing (g) between the components (≈0.98 when $L/g \approx 10^2$). In addition, the environment

DOI: 10.1364/OE.22.0A1604
SOURCE: Optics Express 22, no. S6, A1604, 2014.

and the PV cell are approximated as blackbodies at 300 K; this assumption is appropriate for STPVs that neglect: (i) the fraction of radiation from the absorber that reaches the sun relative to the ambient (which is less than 10% at 3,000x), and (ii) the impact of radiative recombination in the PV cell on the absorber-emitter temperature—we set the fraction of recombination that is radiative, *f*, to 0.1 such that we can neglect this contribution in our analysis. By neglecting these two contributions to the energy balance, we indeed underestimate the STPV performance.

Regarding the parasitic losses, the emittance of the inactive area is set to δ_l of the respective side. The inactive area refers to the absolute difference between the absorber and the emitter areas. For example, if the emitter is larger than the absorber (A_e>A_a), then $\bar{\varepsilon}_{na} = \delta_l^a$, and vice versa. Considering an opposing reflective shield with a reflectance of 0.96 (a reasonable value for a metallic mirror at near-ambient temperatures [21]), the effective emittance of the inactive area ($\bar{\varepsilon}_{na}^{eff}$) can be approximated as [22]:

$$\bar{\varepsilon}_{na}^{eff} = \left[\frac{1}{\delta_l} + \frac{1}{(1-0.96)} - 1 \right]^{-1} \tag{2}$$

The effective emittance is determined by considering radiative exchange between two infinite gray plates. The parasitic loss to the mechanical supports ($Q_{parasitic}$) is assumed to be 5% of thermal emission from the emitter ($0.05Q_e$); this is a reasonable target for a scaled up STPV system as determined using a more detailed model of losses [3].

Once the temperature of the absorber-emitter is determined from the energy balance for a given solar input, our calculation for the amount of electrical power generated by the PV cell follows the Shockley-Queisser analysis [10] and is consistent with previous studies [19, 20]. First, the ultimate power (p_u) generated per unit area of the PV cell is determined by assuming that every photon reaching the cell with energy greater than E_g excites one electron–hole pair, extracted at E_g:

$$p_u = \int_0^{\lambda_g} \varepsilon_\lambda e_{b\lambda} \frac{\lambda}{\lambda_g} d\lambda \tag{3}$$

where $e_{b\lambda}$ is the spectral emissive power:

$$e_{b\lambda} = \frac{2\pi hc^2}{\lambda^5 (\mathrm{e}^{hc/\lambda k_b T} - 1)} \tag{4}$$

The ultimate power is then corrected by two factors [11]: *v*, which accounts for the fact that the open circuit voltage (V_{oc}) is less than the bandgap voltage (V_g=E_g/*q*, where *q* is the electron charge); and *m*, an impedance matching factor:

$$v = \frac{V_{oc}}{V_g} = \frac{k_b T_{PV}}{E_g} \ln\left(f \frac{\int_0^{\lambda_g} R_{\lambda,e} d\lambda}{\int_0^{\lambda_g} R_{\lambda,PV} d\lambda} \right) \tag{5}$$

where k_b is the Boltzmann constant, R_λ is the photon number flux (R_λ is simply $e_{b\lambda}$ divided by hc/λ), and *f* is set to 0.1 as mentioned above. The impedance matching factor (*m*) describes the maximum output power that can be extracted from a single p-n junction cell:

$$m = \frac{z_m^2}{(1 + z_m - e^{-z_m})(z_m + \ln(1 + z_m))} \tag{6}$$

where z_m is qV_{max}/k_bT_{pv} and is determined using the following relation:

$$z_m + \ln(1 + z_m) = \frac{qV_{oc}}{k_b T_{PV}} \tag{7}$$

The actual power generated (*P*) by the STPV is determined using $P = p_u A_{PV} mv$, where A_{pv} is the area of the PV cell (assumed to be equal to the emitter area). Then, *P* can be normalized

DOI: 10.1364/OE.22.0A1604
SOURCE: Optics Express 22, no. S6, A1604, 2014.

by the solar input power (cG_sA_a) to obtain the overall solar-to-electrical conversion efficiency of the STPV system (η_{stpv}). By replacing emission from the emitter with concentrated AM 1.5D irradiation, Eqs (3)-(7) can also be used to determine the efficiency of the PV cell "alone" (*i.e.*, without the additional thermal absorption/emission processes characteristic of STPVs); thus providing a justifiable framework for STPV vs. PV efficiency comparisons. Our PV model follows the Shockley-Queisser analysis [10] expect that it considers a concentrated AM 1.5D spectrum and f is set to 0.1.

3. Optimization of efficiency

This section uses the model described above to discuss the optimal STPV efficiency over a range of optical concentrations (1-3,000x), and bandgaps (0.45-0.80 eV). From an engineering perspective, it is envisioned that the level of optical concentration and the choice of PV cell will likely be determined by factors such as cost, availability, system size, *etc*. Thus, these two parameters were allowed to vary. To determine the design which maximized the overall STPV efficiency at each operating point, the following parameters were simultaneously optimized: the temperature of the absorber-emitter, the emitter-to-absorber area ratio, the absorber-side cutoff wavelength (note: the emitter-side cutoff is fixed by the bandgap of the PV). The impact of non-idealities on the optimal parameters within the considered design space will be discussed in more detail in the following sub-sections.

Although in theory the optical concentration can exceed 45,000x, we are more interested in optical concentrations commonly used in terrestrial solar thermal applications (typically below 3,000x). Regarding the range of bandgaps, the analysis described in this section can easily be extended to larger PV bandgaps such as that of silicon. However, considering the current level of non-idealities, reaching high efficiencies with larger bandgaps would require high levels of optical concentration, as well as operating temperatures that are high considering the thermal stability of nanostructured surfaces.

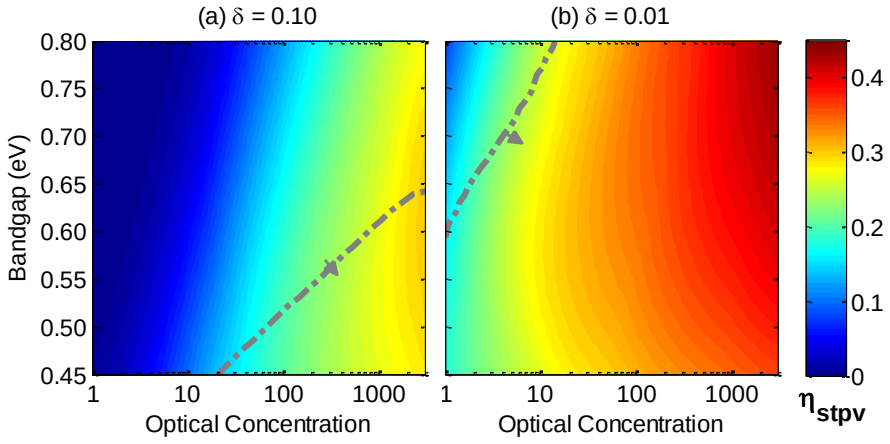

Fig. 3. Optimized STPV efficiency in the presence of (a) 0.10 and (b) 0.01 non-idealities (δ). Design space covers a range of bandgaps and optical concentrations. Each operating point corresponds to a specific absorber-side cutoff [Fig. 4], absorber-emitter temperature [Fig. 5], and emitter-to-absorber area ratio [Fig. 6]. Arrow points to region where the STPV efficiency exceeds the PV efficiency (same cell as in STPV) as delineated by the dash-dot line.

The optimal STPV efficiency for a system with 0.10 and 0.01 non-ideality (δ) is shown in Figs. 3(a) and 3(b), respectively. In general, the STPV efficiency increases strongly with increasing optical concentration at a fixed bandgap. On the other hand, we observe an optimal E_g at a fixed concentration which balances PV losses (characteristic of low E_g) with thermal re-radiation losses (associated with the high temperatures needed with increasing E_g). Figure 3

DOI: 10.1364/OE.22.0A1604
SOURCE: Optics Express 22, no. S6, A1604, 2014.

also shows where the STPV efficiency exceeds the efficiency of the PV cell alone (under solar illumination); in this region, adding an absorber-emitter is beneficial. By decreasing the level of non-idealities from 0.10 to 0.01, the STPV efficiency begins to exceed the PV efficiency and to reach relatively high efficiencies at more moderate optical concentrations (*i.e.*, > 34% efficiency at 100x). However, to achieve 0.01 non-idealities, additional components such as selective windows and filters or absorber-emitter surfaces with much better spectral control are needed.

3.1 Absorber-side cutoff wavelength optimization

A cutoff wavelength is where the absorber-side properties transition from high emittance at shorter wavelengths, needed to absorb and thermalize sunlight, to low emittance at longer wavelengths, needed to suppress thermal re-emission from the absorber. The cutoff wavelength on the absorber-side maximizes the amount of solar energy collected as heat (see Appendix A for details).

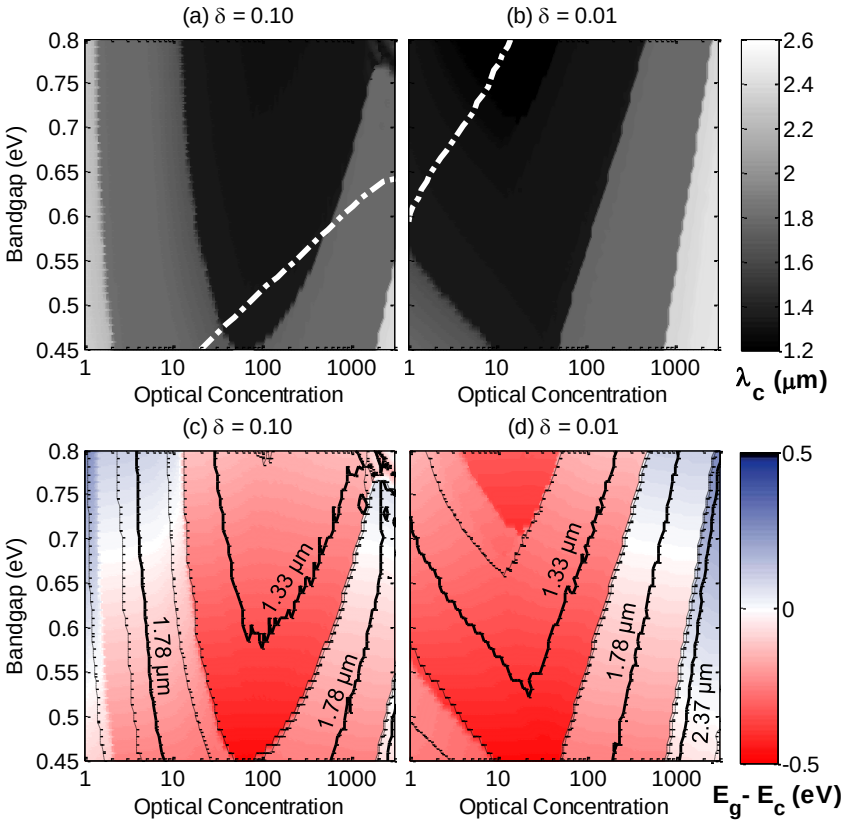

Fig. 4. Optimal absorber-side cutoff wavelength (λ_c) for an STPV with (a) 0.10 and (b) 0.01 non-idealities. Dash-dot line [see Fig. 3] delineates the region where STPV efficiency exceeds the PV efficiency. (c) and (d) λ_c plotted as energy (E_c) relative to the PV bandgap energy (E_g), corresponding to (a) and (b) respectively. Thick black contours represent the median cutoff wavelength for each cluster from Appendix A with the corresponding 10/90 percentile of each cluster [see Fig. 13] shown with thin contours. Note: the emitter-side cutoff is set to the bandgap energy.

Despite the fact that they are separated by a vacuum gap, we can consider the window and the absorber as part of one absorber-side unit whose goal it is to create this spectral selectivity (*i.e.*, allow sunlight to get absorbed while suppressing thermal emission from leaving the unit). Figures 4(a) and 4(b) show the ideal cutoff wavelengths that optimize the STPV

DOI: 10.1364/OE.22.0A1604
SOURCE: Optics Express 22, no. S6, A1604, 2014.

efficiencies shown in Figs. 3(a) and 3(b), respectively. In general, λ_c increases with increasing optical concentration since the solar flux begins to dominate the thermal emission in the near-IR, shifting λ_c to longer wavelengths. By comparing Figs. 4(a) and 4(b), the optimal cutoff wavelengths are shifted to lower concentrations by decreasing the non-idealities to 0.01. This trend of shifting of the optimal parameters to lower concentrations with a reduction of non-idealities is consistent with the trend for efficiency [see Fig. 3]. Below ~10 suns in the 0.10 non-ideality case, however, λ_c increases with decreasing optical concentration because the design struggles to reach high enough temperatures for efficient operation. Nonetheless, this regime is not of practical interest since the efficiency is degraded relative to a PV cell.

There are specific bands of sunlight that are attenuated due to atmospheric absorption which lead to clustering of the cutoff wavelengths at the high-energy edge of the atmospheric bands of the AM 1.5D spectrum. Due to these absorption bands, we can group the optimal cutoffs into three wavelength ranges 1.30-1.34 μm (short), 1.71-1.79 μm (medium), and 2.25-2.47 μm (long) with a respective median of 1.33 μm, 1.78 μm and 2.37 μm as shown in Figs. 4(c) and 4(d). Each of these median cutoff wavelengths is best suited for a particular band of operating points. Here we have plotted the absorber-side cutoff wavelength as a cutoff energy ($E_c=\lambda_c/hc$) relative to the bandgap energy (E_g). *Red* corresponds to regions where the bandgap is red-shifted relative to the cutoff energy. In contrast, *blue* corresponds to regions where the bandgap is blue-shifted relative to the cutoff energy. The latter does not imply energy up-conversion because the mean energy of the solar irradiation is still higher than the mean energy of the thermal emission. Nevertheless, this analysis can be extended to higher bandgap PV cells to investigate potentially realistic regions where thermally-driven energy up-conversion is achievable [23]. The white regions are also interesting because the cutoff energy matches the bandgap energy. Here, the absorber-side spectral design can potentially double as the emitter-side spectral design such that one spectral control strategy may serve two purposes.

3.2 Temperature optimization

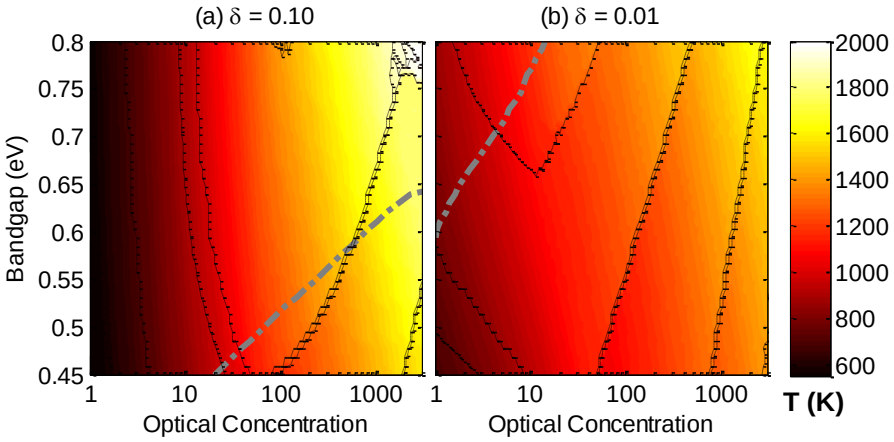

Fig. 5. Optimal temperature of the absorber-emitter for an STPV with (a) 0.10 non-idealities, compared to an STPV with (b) 0.01 non-idealities. Dash-dot line [see Fig. 3] delineates the region where STPV efficiency exceeds the PV efficiency. Thin contours represent the 10/90 percentile of each λ_c cluster [see Fig. 4].

The optimal temperature of the absorber-emitter as a function of concentration and bandgap is shown in Fig. 5. The ideal temperature for the case with 0.10 non-idealities has a stronger dependence on the concentration and the PV bandgap. As the spectral performance improves (0.01 non-idealities), the efficiency is less sensitive to temperature which leads to a more uniform optimal temperature distribution across the design space.

DOI: 10.1364/OE.22.0A1604
SOURCE: Optics Express 22, no. S6, A1604, 2014.

At the boundaries of the λ_c bands, there are abrupt transitions in the optimal temperature. For example, two points that are close in parametric space might see a shift from a medium cutoff (1.78 μm) to a longer cutoff wavelength (2.37 μm) with a corresponding 50-100 K drop in optimal temperature.

3.3 Geometric optimization

Geometrical parameters, such as the size of the emitter relative to the absorber, can be used to achieve optimal performance at a specific solar irradiance or optical concentration. With unconcentrated or low optically-concentrated solar radiation, thermal concentration [24, 25] boosts the hot-side temperature, enabled by low-emittance spectrally-selective surfaces. When high optically-concentrated solar radiation is available, high conversion efficiency is achieved through thermal spreading (high emitter-to-absorber area ratios [3]), enabled by high-absorptance surfaces. Both strategies have been experimentally implemented to achieve substantial improvements (3-8x) in conversion efficiency compared to prior solar-heated thermophotovoltaic [2] (TPV) and thermoelectric [26] (TE) generators.

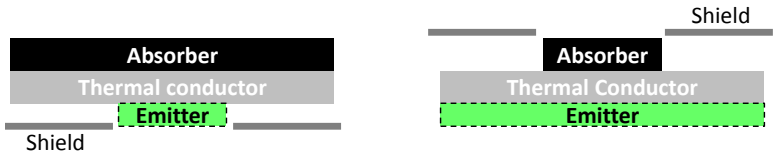

Fig. 6. Geometrical optimization of the size of emitter with respect to the absorber (*AR*): (a) Emitter is smaller than the absorber (*AR*<1), (b) Emitter is larger than the absorber (*AR*>1).

Here we consider more generally the emitter-to-absorber area ratio (*AR*) as a free parameter used for optimization of the overall STPV performance. The low *AR* and high *AR* envisioned devices are shown Fig. 6. As mentioned in the model, a reflecting radiation shield is used to limit the losses from the mismatched areas.

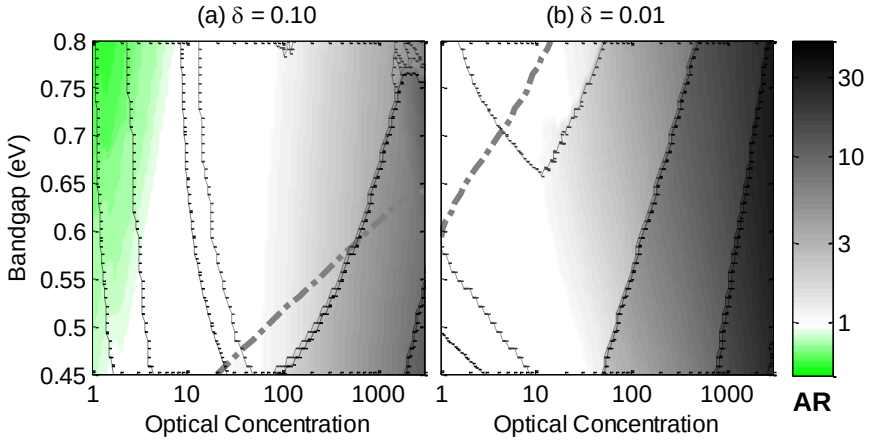

Fig. 7. Optimal absorber-emitter geometry (emitter-to-absorber size, *AR*) for an STPV with (a) 0.10 non-idealities, compared to an STPV with (b) 0.01 non-idealities. Dash-dot line [see Fig. 3] delineates the region where STPV efficiency exceeds the PV efficiency. Thin contours represent the 10/90 percentile of each λ_c cluster [see Fig. 4].

The optimal area ratio as a function of optical concentration and bandgap is shown in Fig. 7. In general, the optimal *AR* increases with concentration. Reducing the size of the absorber decreases the area for re-emissive thermal losses and increases the efficiency of solar collection. The high concentration regime pushes λ_c to longer wavelengths such that it coincides or surpasses λ_g [*i.e.*, the blue-shifted regime in Fig. 4]. However, the high area ratio

DOI: 10.1364/OE.22.0A1604
SOURCE: Optics Express 22, no. S6, A1604, 2014.

regime requires higher levels of optical concentration and effective thermal spreading between the absorber and the emitter to maintain near-isothermal operation.

There is also a regime where thermal concentration is optimal (*AR < 1*), albeit with low efficiency relative to the PV cell. The issue with relying on thermal concentration to achieve these high operating temperatures is that the emissive losses from the large absorber area begin to dominate. Additionally, the parasitic losses from the inactive areas contribute to making efficient thermal concentration difficult to achieve without exceptionally low levels of spectral non-idealities. This effect was previously observed [27], hence, in addition to wavelength selectivity, angular selectivity has been suggested [23, 27] to enable the use of unconcentrated sunlight.

4. Relative importance of emitter-side non-idealities

Thus far, we have explored the impact of uniformly improving the spectral performance from $\delta = 0.10$ to $\delta = 0.01$ on the efficiency at moderate optical concentrations, as well as the optimal temperature, cutoff wavelength and area ratio. Instead of uniformly decreasing the non-idealities on the emitter side, we consider the impact of independently increasing the below-λ_g emittance ($1\text{-}\delta_h^e$) from 0.90 to 0.99 and decreasing the emittance above-λ_g (δ_l^e) from 0.10 to 0.01 [see Fig. 8(a)]. Figure 8(b) shows the boost in efficiency at a specific bandgap (0.55 eV) for each of the spectral improvements. Increasing the below-λ_g has a negligible effect on the efficiency. On the other hand, decreasing the above-λ_g emittance increases the efficiency significantly; a 0.09 decrease in emittance consistently increases the efficiency by ~5% (absolute) at moderate and high optical concentrations.

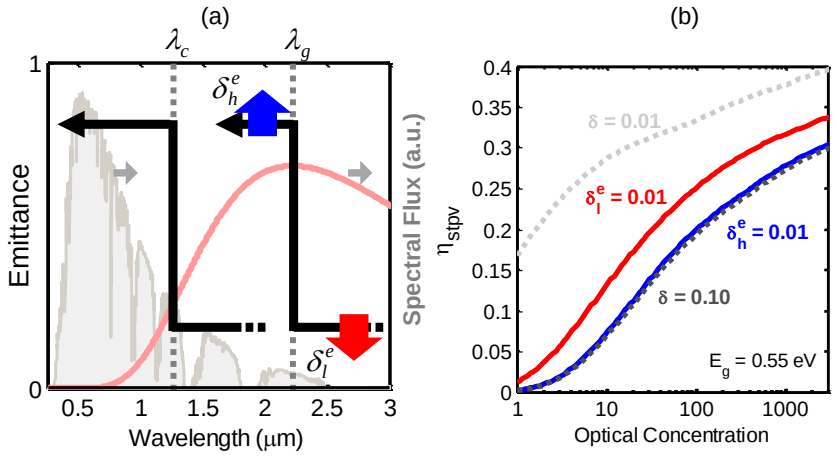

Fig. 8. The impact of independently increasing the emitter-side emittance below λ_g (*blue*) as compared to decreasing the emittance above λ_g (*red*), schematically shown in (a), on the STPV efficiency (b). $\delta = 0.10$ is the baseline case.

To understand the reason decreasing the above-λ_g non-ideality has a much stronger impact on the efficiency, we compare the emissive power above and below λ_g at the optimal operating point. This ratio is termed the emitter-side weighting parameter (W_e):

$$W_e = \frac{e_{\lambda>\lambda_g}}{e_{\lambda<\lambda_g}} \tag{8}$$

where e is the emissive power within the range specified by the subscript. As shown Figs. 9(a) and 9(b), $W_e > 1$ for a 0.55 eV bandgap over the entire range of concentrations considered. This implies that the emissive power above λ_g is much greater than below λ_g, by as much as one or two orders of magnitude depending on the operating point. The emissive power is

DOI: 10.1364/OE.22.0A1604
SOURCE: Optics Express 22, no. S6, A1604, 2014.

greater above λ_g because increasing the temperature is detrimental to the absorber efficiency and it also increases losses associated with thermalization as it blue-shifts the emitted power content relative to the bandgap, where the spectral response is lower. For these reasons, the power content above λ_g is high and any deviation from ideality results in a large direct loss. This observation explains why the efficiency is drastically improved when the emittance above λ_g (*i.e.*, at energies below E_g) is decreased.

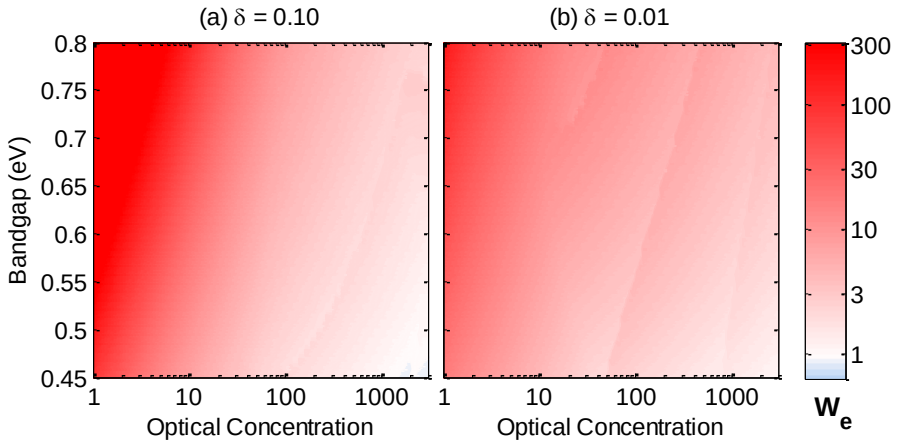

Fig. 9. Emitter-side weighting parameter W_e for an STPV with (a) 0.10 compared to (b) 0.01 non-idealities.

The fact that W_e is still high in the high spectral performance case [Fig. 9(b)] suggests that efforts should be focused on suppressing or recycling sub-bandgap radiation even further. Thus, in addition to having a low emittance substrate as the emitter, the following components will be beneficial: a filter that allows useful radiation to pass while reflecting long-wave radiation and a reflector on the backside of the PV cell. By using all three approaches, the STPV efficiencies can be significantly improved. Care should of course be taken not to seriously degrade the useful thermal emittance ($\lambda<\lambda_g$) because of the power density considerations mentioned previously. We also re-iterate that our analysis only considers a single cutoff wavelength (λ_g). Further improvements in efficiency could be achieved using an emittance profile with a double-sided cutoff (*i.e.*, a narrow-band emitter) to limit losses associated with thermalization in the PV cell.

5. Relative importance of absorber-side non-idealities

Similar to the above analysis, we can consider the relative importance of increasing the solar absorptance (at wavelengths below λ_c) to that of decreasing the thermal emittance (at wavelengths above λ_c) as shown in Fig. 10(a). The increase in efficiency when the emittance below λ_c ($1\text{-}\delta_h^a$) is independently increased from 0.90 to 0.99 (in *blue*), and when the emittance above λ_c (δ_l^a) is independently decreased from 0.10 to 0.01 (in *red*) are shown in Fig. 10(b). The improvement in efficiency can be as high as 5-10 absolute percentage points due to each of the spectral improvements, depending on the optical concentration and the operating regime.

DOI: 10.1364/OE.22.0A1604
SOURCE: Optics Express 22, no. S6, A1604, 2014.

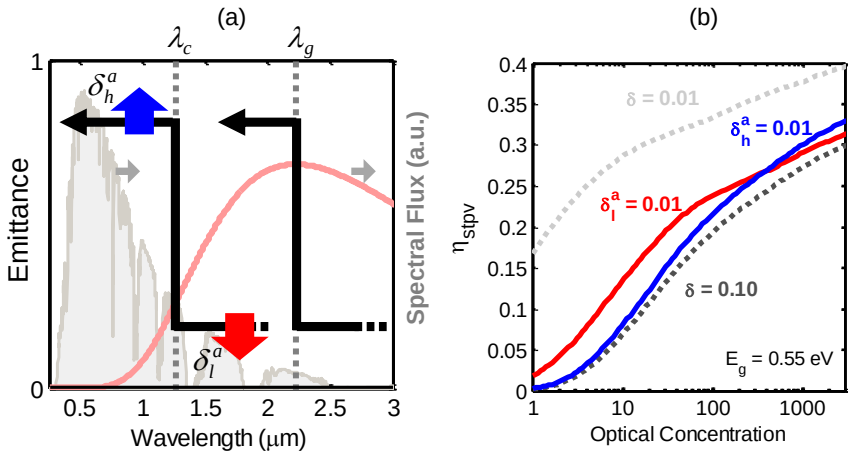

Fig. 10. The impact of independently increasing the absorber-side solar absorptance (blue) as compared to decreasing the thermal emittance (red), schematically shown in (a), on the STPV efficiency (b). The baseline case has uniform spectral non-idealities (δ = 0.10).

The cross-over is explained by comparing the incident solar flux (cG_s) to the emissive flux (σT^4). This ratio is termed the absorber-side weighting parameter (W_a):

$$W_a = \frac{\sigma(T_{ae}{}^4 - T_{amb}^4)}{cG_s} \tag{9}$$

Figures 11(c) and 11(d) show W_a at the optimal design. There is indeed a $W_a < 1$ regime where the incident solar flux dominates (in *blue*), and a $W_a > 1$ regime where the emissive flux dominates (in *red*). The absorber-side weighting parameter explains the cross-over behavior in efficiency and the existence of two distinct regions: a low W_a regime where high absorptance is more important and a high W_a regime where low emittance is more important. If the solar flux dominates, then increasing the absorptance below the cutoff wavelength is beneficial; on the other hand, if the emissive flux dominates, then decreasing the emittance above the cutoff wavelength is more beneficial.

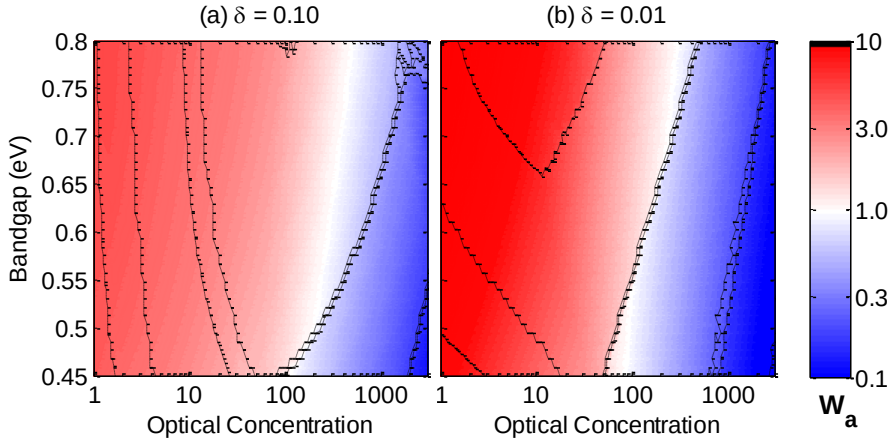

Fig. 11. Absorber-side weighting parameter for an STPV with (c) 0.10 compared to (d) 0.01 non-idealities. Thin contours represent the 10/90 percentile of each λ_c cluster [see Fig. 4].

It is interesting to note that W_a can be obtained by re-arranging the energy balance [Eq. (1)] on the absorber-emitter:

DOI: 10.1364/OE.22.0A1604
SOURCE: Optics Express 22, no. S6, A1604, 2014.

$$W_a = \frac{\sigma(T_{ae}{}^4 - T_{amb}{}^4)}{cG_s} = \frac{\bar{\alpha}_{abs}}{\bar{\varepsilon}_{abs} + \bar{\varepsilon}_{emit} \cdot AR + parasitic} \quad (10)$$

After re-arranging the equation, we observe that the area ratio and the parasitic losses appear in the denominator. Thus, with increasing area ratio and/or parasitic losses, we expect the solar flux to increase and dominate over the thermal emission. This result explains the coupling between the relative importance of spectral non-idealities and the area ratio, and by extension, the optimal cutoff wavelength (as previously mentioned).

This information is valuable as a guide for spectral engineering and materials selection. Even within each band of cutoff wavelengths, we observe a subtle transition from $W_a > 1$ to $W_a < 1$, suggesting that the cutoff wavelength does not fully specify which selective surface is best suited for a particular operating point. For example, two surfaces that have the same cutoff wavelength but different absorptance/emittance values might perform better under different operating conditions.

6. Discussion

Not all of the wavelengths above or below a cutoff have the same impact on the performance. By extension to our analysis on weighting parameters, the regions with the highest spectral flux are expected to have the largest impact on the efficiency. On the emitter side, the highest flux typically occurs near the bandgap making near-λ_g spectral properties and the sharpness of the cutoff very important. On the absorber side, the net spectral flux [see Fig 12(a)] is near zero at the cutoff wavelength, making near-λ_c properties and the sharpness of the cutoff less important. A more spectrally-resolved weighting parameter can be developed to capture these effects. Our framework can also be easily modified to consider the impact of non-idealities in near-field TPV conversion.

7. Conclusion

We investigated the design of solar thermophotovoltaics (STPVs) in the presence of spectral non-idealities and parasitic losses. The detailed-balance analyis was modified to account for the actual AM 1.5D solar spectrum, spectral non-idealities, and parasitic losses. This model was used to maximize STPV efficiency over a range of PV bandgaps (0.45-0.80 eV) and optical concentrations (1-3,000x) by determining the optimal temperature, emitter-to-absorber area ratio (*AR*) and absorber cutoff wavelength at each operating point. The impacts of non-idealities on the efficiency and the optimal parameters were investigated. The results are explained using dimensionless parameters weighting the relative importance of non-idealities on the emitter-side and the absorber-side. On the emitter-side, we show that emissive power above λ_g dominates (W_e>1) such that suppressing or recycling sub-bandgap radiation is critical. On the absorber side, the relative strength of thermal emissive power to solar irradiance (W_a) depends on the operating regime such that re-emissive (absorptive) non-idealities are generally more important at low (high) concentrations. Due to the atmospheric absorption bands in the AM 1.5D spectrum there are three prevalent absorber-side cutoff wavelengths, each of them coupled to a specific regime: 1.33 μm (*AR*≈1, W_a≈0.1-1), 1.78 μm (*AR*≈1-10, W_a≈1-10) and 2.37 μm (*AR*≈10-100, W_a≈10-100). These parameters can be used to construct a physically meaningful figure of merit when calculating the optimal surface nanostructure using an electromagnetic solver, or vice versa, to determine what device design and operating regime are best suited for a particular selective surface. In general, the framework developed here can be used as a guide for materials selection and targeted spectral engineering in STPVs.

DOI: 10.1364/OE.22.0A1604
SOURCE: Optics Express 22, no. S6, A1604, 2014.

8. Appendix A: Absorber-side cutoff wavelength

In the simple case where the solar spectrum is approximated by a blackbody at 5800 K and the selective surface transitions from ideal absorptance to zero emittance, the cutoff wavelength is defined by the intersection of the incident spectral flux (set by the optical concentration) and the thermal emissive flux outgoing from the surface (set by the temperature). Here we consider a slightly more complex case where the actual AM 1.5D spectrum is considered, and non-idealities are introduced above and below the cutoff. The net spectral flux (solar incoming minus thermal outgoing) is shown in Fig. 12(a). Because of the discrete nature of the AM 1.5D spectrum, multiple wavelengths could exists where the net flux is zero, meaning the thermal flux (Q_λ) equals the solar flux (H_λ). Nevertheless, there is typically only one cutoff wavelength that maximizes the amount of heat collected by the absorber-side. This cutoff is more rigorously determined by integrating the net spectral flux up to a given wavelength, as shown in Fig. 12(b). The ideal cutoff wavelength corresponds to the maximum point along this curve.

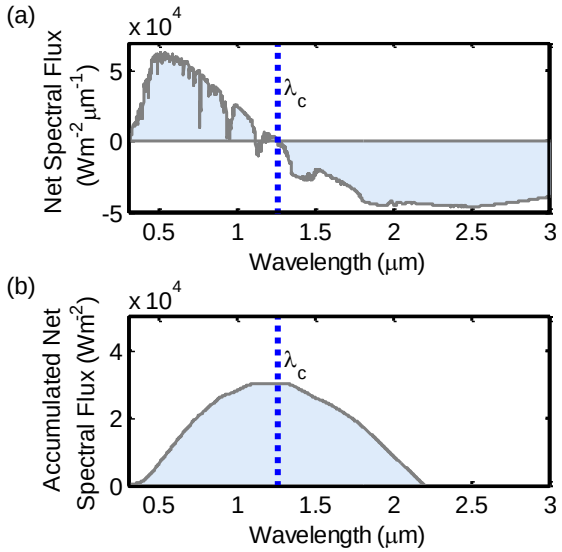

Fig. 12. Optimization of the absorber-side cutoff wavelength. Net spectral flux (a) integrated up to a wavelength of interest (b). Optimal cutoff wavelength shown.

Even though we have determined the cutoff wavelength by assuming ideal absorptance at wavelengths below the cutoff and zero emittance above the cutoff, the methodology is general. The assumption of ideality allowed us to represent the accumulated net flux (or heat collected) with a simple integral of H_λ -Q_λ up to the wavelength of interest:

$$\int_0^{\lambda} \left(H_{\lambda'} - Q_{\lambda'} \right) d\lambda' \tag{11}$$

The question naturally arises whether or not this cutoff wavelength optimizes the collected sunlight when spectral non-idealities are introduced. It can be mathematically shown that by introducing spectral non-idealities, the new function to be optimized is a scaled and vertically translated version of the original accumulation function, taking on the following form:

$$C_1 \left(\int_0^{\lambda} H_{\lambda'} - Q_{\lambda'} d\lambda' \right) + C_2 \tag{12}$$

where C_1 and C_2 are wavelength-independent constants:

$$C_1 = 1 - \delta_l^a - \delta_h^a$$

DOI: 10.1364/OE.22.0A1604
SOURCE: Optics Express 22, no. S6, A1604, 2014.

$$C_2 = \delta_l^a \left[cG_s - \sigma(T_{ae}{}^4 - T_{amb}^4) \right] \tag{13}$$

Therefore, as long as the emittance below the cutoff is larger than the emittance above the cutoff (and the cutoff is perfectly sharp), the cutoff wavelength determined using the accumulation methodology is universal.

The only parameters determining the optimal cutoff wavelength are the optical concentration and the temperature of the absorber, and of course, the solar spectrum of interest. In the case of AM 1.5D, there are specific bands of sunlight that are attenuated due to atmospheric absorption. These spectral features lead to clustering of the cutoff wavelengths at the high-energy edge of the atmospheric bands, as shown in Fig. 13. From the median of each cluster, we can determine the three most prevalent cutoff wavelengths: 1.33 μm, 1.78 μm and 2.37 μm.

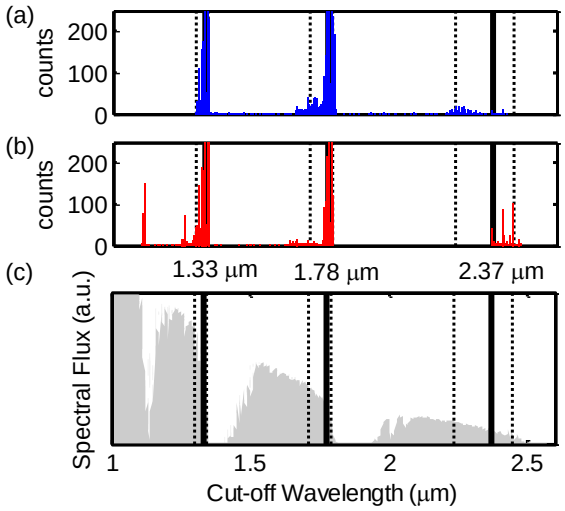

Fig. 13. Grouping of absorber-side cut-off wavelengths. Histogram of optimal cutoff wavelengths corresponding to Fig. 3 for (a) 0.10 and (b) 0.01 non-ideality cases. (c) AM 1.5D spectral flux (gray) with the median cutoff wavelength (solid black) for each cluster and its corresponding 10/90 percentile (dashed lines).

Acknowledgments

This work is supported as part of the Solid-State Solar Thermal Energy Conversion (S3TEC) Center, an Energy Frontier Research Center funded by the U.S. Department of Energy, Office of Science, Office of Basic Energy Sciences under DE-FG02-09ER46577. The authors acknowledge J. Chou, V. Rinnerbauer, and A. Veeraragavan for helpful discussions. Y.N. acknowledges the support from Space Core Technology Program through the National Research Foundation of Korea (NRF) funded by the Ministry of Science, ICT & Future Planning (No. 2014M1A3A3A02034818).